

A new outburst of the yellow hypergiant star ρ Cas

M. Kraus^{1*}, I. Kolka², A. Aret^{1,2}, D. H. Nickeler¹, G. Maravelias^{3,4}, T. Eenmäe²,
A. Lobel⁵, V. G. Klochkova⁶

¹ *Astronomický ústav, Akademie věd České republiky, Fričova 298, 251 65 Ondřejov, Czech Republic*

² *Tartu Observatory, University of Tartu, 61602 Tõravere, Tartumaa, Estonia*

³ *IESL, Foundation for Research and Technology-Hellas, 100 Nikolaou Plastira Street, 71110 Heraklion, Crete, Greece*

⁴ *Physics Department, University of Crete, P.O. Box 2208, 71003 Heraklion, Crete, Greece*

⁵ *Royal Observatory of Belgium, Ringlaan 3, 1180, Brussels, Belgium*

⁶ *Special Astrophysical Observatory of the Russian Academy of Sciences, Nizhnii Arkhyz 369167, Russia*

Accepted XXX. Received YYY; in original form ZZZ

ABSTRACT

Yellow hypergiants are evolved massive stars that were suggested to be in post-red supergiant stage. Post-red supergiants that evolve back to the blue, hot side of the Hertzsprung-Russell diagram can intersect a temperature domain in which their atmospheres become unstable against pulsations (the Yellow Void or Yellow Wall), and the stars can experience outbursts with short, but violent mass eruptions. The yellow hypergiant ρ Cas is famous for its historical and recent outbursts, during which the star develops a cool, optically thick wind with a very brief but high mass-loss rate, causing a sudden drop in the light curve. Here we report on a new outburst of ρ Cas which occurred in 2013, accompanied by a temperature decrease of ~ 3000 K and a brightness drop of 0.6 mag. During the outburst TiO bands appear, together with many low excitation metallic atmospheric lines characteristic for a later spectral type. With this new outburst, it appears that the time interval between individual events decreases, which might indicate that ρ Cas is preparing for a major eruption that could help the star to pass through the Yellow Void. We also analysed the emission features that appear during phases of maximum brightness and find that they vary synchronous with the emission in the prominent [Ca II] lines. We conclude that the occasionally detected emission in the spectra of ρ Cas, as well as certain asymmetries seen in the absorption lines of low to medium-excitation potential, are circumstellar in nature, and we discuss the possible origin of this material.

Key words: stars: massive — supergiants — stars: atmospheres — stars: individual: ρ Cas

1 INTRODUCTION

Yellow Hypergiants (YHGs) are cool ($T_{\text{eff}} = 4000\text{--}7000$ K), luminous ($5.4 \leq \log L/L_{\odot} \leq 5.8$) massive stars. de Jager (1998) proposed that these objects evolve to the blue, hot side of the Hertzsprung–Russell (HR) diagram after having passed through the red supergiant (RSG) phase (de Jager 1998). Despite the fact that they are amongst the visually brightest objects, YHGs are rare, indicating that this phase is short. Nevertheless, these objects are cornerstones in the evolution of massive stars, because they link the cool RSGs and the hot pre-supernova stages such as Luminous Blue Variables and Wolf-Rayet stars.

When the stars enter the temperature regime between

7000 and 11000 K, which is referred to as the ‘Yellow Evolutionary Void’ (de Jager 1998) or ‘Yellow Wall’ (Oudmaijer et al. 2009), their atmospheres start to become dynamically unstable and strong mass loss sets in (Nieuwenhuijzen & de Jager 1995; de Jager & Nieuwenhuijzen 1997; Stothers & Chin 2001). Moreover, when approaching this instability domain the stars may shed their outer layers in a series of outbursts denoted as ‘bouncing against the Yellow Void’ (de Jager & Nieuwenhuijzen 1997). These outbursts can result in the formation of multiple detached shells such as the double-shell structure detected on mid-infrared images of the post-RSG star IRAS 17163-3907 (the ‘Fried Egg’ nebula, Lagadec et al. 2011), or the ejecta resolved on HST images around the YHG star IRC +10420 (Tiffany et al. 2010). During an outburst event, the star appears dimmer, hence cooler so

* E-mail: michaela.kraus@asu.cas.cz

Table 1. Observation log of the Ondřejov spectra

Date	JD	T _{Exp} (H α) (s)	T _{Exp} ([Ca II]) (s)	T _{Exp} (Ca II trip.) (s)
2010-07-17	2455394	600	—	1800
2011-03-06	2455627	900	1100	—
2011-04-18	2455669	300	300	—
2011-08-21	2455795	900	800	—
2011-08-24	2455797	—	—	600
2011-09-04	2455809	600	1200	900
2011-09-06	2455811	—	900	—
2011-09-11	2455816	1300	800	—
2011-09-12	2455816	—	—	1580
2011-09-15	2455819	900	1000	1200
2011-09-23	2455828	—	1800	—
2011-09-24	2455828	1200	—	—
2011-10-15	2455850	1800	1800	1800
2011-11-06	2455872	900	1200	1800
2012-07-28	2456136	200	300	1200
2012-08-03	2456143	800	600	1000
2012-09-28	2456199	900	800	1174
2013-06-27	2456471	1200	—	—
2013-06-28	2456471	—	1200	—
2013-10-01	2456567	1200	1800	1800
2014-07-19a	2456857	300	—	—
2014-07-19b	2456858	300	750	1200
2014-10-28	2456959	2400	3000	6000
2014-12-13	2457005	900	—	—
2015-01-13	2457036	900	2600	—
2015-02-06	2457060	3600	3600	—
2015-03-19	2457100	600	900	1200
2015-06-04	2457178	600	—	—
2015-06-05	2457178	—	900	900
2015-06-12	2457186	1100	—	—
2015-06-13	2457186	—	700	700
2015-06-17	2457191	1500	—	—
2015-06-26	2457199	600	600	600
2015-07-09	2457213	1200	900	1200
2015-07-20	2457224	400	400	400
2015-11-24a	2457350	1200	—	—
2015-11-24b	2457351	800	1200	1300

that the object evolves on an apparent red loop in the HR diagram.

The proposed bouncing might continue until a significant part of the outer shell is lost and the stellar atmosphere finally becomes stable again and the star might appear on the blue side of the Yellow Void where it could continue its life as a blue supergiant of α Cygni-type variable or as a Luminous Blue Variable. Alternatively, if its mass-loss behaviour has changed from spherically to axis-symmetrically, as it seems to be the case for IRC +10420 (Davies, Oudmaijer & Sahu 2007) and possibly also for V509 Cas (Aret et al. 2017b), the star might also appear as B[e] supergiant.

YHG's hence occupy a critical phase in the evolution of massive stars, and the mass loss during this phase is crucial for the fate of the object. For a better comprehension of the physics that control the atmospheric dynamics and eventually lead to mass eruptions in YHG's, as well as to catch phases of mass ejections, monitoring these stars is essential. Here, we report on the discovery of a new outburst in ρ Cas, which is one of the northern Galactic YHG's that we monitor since 2010.

2 THE OBJECT

The YHG star ρ Cas (HD 224014) is famous for its historical and recent outbursts, and at least three have been recorded so far. The first major outburst occurred in 1945–1947 and was discovered by Popper¹ (1946), who reported on the deep minimum in 1946. Another one took place in 2000–2001 (Lobel et al. 2003) and was henceforth referred to as the Millennium outburst. Each of these major outbursts was accompanied by a drop in the light curve by more than one magnitude. A third, less violent incident was noted in 1985–1986 (Boyarchuk, Boyarchuk & Petrov 1988b), during which the brightness dimmed by only about 0.6–0.7 mag. During every event TiO absorption bands arose in the optical and near-infrared stellar spectra (Popper 1947; Thackeray 1948; Boyarchuk et al. 1988b; Lobel et al. 2003), indicative for the development of a cool, optically thick wind with a high mass-loss rate.

Dust with a temperature of about 600 K was detected with IRAS in 1983 consistent with an optically thin dust shell formed from the ejected material during the 1946 outburst (Jura & Kleinmann 1990). Recent mid-infrared photometric observations by Shenoy et al. (2016) confirm the expansion and thinning of this dust shell, while no indication for new dust formation following the millenium outburst was found yet. Also, no evidence for extended emission resulting from previous mass-loss episodes during the RSG phase was found in deep *Hubble Space Telescope* images (Schuster, Humphreys & Marengo 2006).

During the quiescence phases, ρ Cas shows line-profile and low-amplitude photometric variability that is ascribed to semi-regular pulsations (Sheffer & Lambert 1986) with a quasi-period of 300 d and a corresponding brightness fluctuation of 0.2 mag (Zsoldos & Percy 1991). These pulsations manifest themselves also in an excess line broadening of the photospheric lines. Pure radial pulsations as cause of the temperature and radial velocity variation have been ruled out (Lobel et al. 1994), and de Jager (1998) proposed that ρ Cas pulsates in a combination of both pressure and gravity modes.

Over the pulsation cycles, ρ Cas displays effective temperature oscillations between 500 K (Israeli, Lobel & Schmidt 1999) and 750 K (Lobel et al. 1998), although slightly larger values have recently been reported as well (Klochkova et al. 2014). Moreover, the temperature follows very tightly the variations of the light curve, also during the outbursts (Lobel et al. 2003).

Occasionally, numerous and prominent emission lines arise in the optical and infrared spectral regions. These appearances were found to be synchronized with phases of maximum light corresponding to periods of fast expansion of the atmosphere (see, e.g., Lobel et al. 2003; Gorlova et al. 2006; Yamamuro et al. 2007). The molecular features of the CO first-overtone bands arising in the near-infrared longward of 2.3 μ m seem to be most sensitive. These bands change from intense emission to strong absorption on a time-scale of weeks to months. An explanation for their occurrence is, however, controversial: Gorlova et al. (2006) place

¹ D. M. Popper, Harvard Announcement Card, No. 752, 1946; for the light curve see Beardsley (1961).

the CO band formation region in the vicinity of the pulsating photosphere and correlate their variability with the pulsation cycles, whereas Yamamuro et al. (2007) propose the CO band formation to be related to a mass-loss event in which the change from emission to absorption is due to the expansion of the ejected gas shell. Some emission lines in the spectrum of ρ Cas seem to be always present, such as the [CaII] lines, (e.g., Lobel et al. 2003; Aret et al. 2017a), which are proposed to form in a circumstellar gas shell.

A further peculiarity in the spectra of ρ Cas is the appearance of split lines. The origin of these lines is still controversial. Lobel et al. (1998) identify two types of split lines: in one type a static emission of the same transition superimposes the broad, cyclically variable absorption component. This splitting is observed in the cores of the absorption components of neutral and ionized metallic lines. These lines have typically (very) low excitation energies, and the static emission is proposed to form in an outer envelope (Lobel et al. 1994) or tenuous, diffuse circumstellar gas shell (Lobel et al. 1998). A second type of split lines arises from the superposition of an emission line on the highly variable absorption profile of a different transition, causing an apparent split of the absorption line. A superimposed circumstellar emission component was also the preferred explanation for the split lines seen by Gorlova et al. (2006).

However, alternative scenarios were suggested as well. For instance, Gesicki (1992) interpreted the split lines as due to two superimposed absorption components of which the red one originates within the photosphere of ρ Cas, whereas the blue component forms in a hot, expanding circumstellar envelope. Support for such a scenario was found by Klochkova et al. (2014) and Klochkova et al. (2018) based on a comparison of the dynamics from symmetric, non-distorted absorption lines and from permanently split lines. Although the star has been subject to many studies and detailed analyses throughout the past century, its atmospheric dynamics causing unusually broad photospheric absorption lines, peculiar and strongly variable emission line spectra, recurring massive outburst events, pulsation properties, and characteristics of its circumstellar environment still remain elusive.

3 OBSERVATIONS

We spectroscopically monitored ρ Cas between 2010 July 16 and 2015 November 24. The observations were obtained using the Coudé spectrograph (Slechta & Skoda 2002) attached to the Perek 2-m telescope at Ondřejov Observatory. Until the end of May 2013, the observations were taken with the 830.77 lines mm^{-1} grating and a SiTe 2030 \times 800 CCD. Beginning in June 2013, we used the newly installed PyLoN 2048 \times 512BX CCD. The spectra were taken in three different wavelength regions: 6250–6760 Å, 6990–7500 Å, and 8470–8980 Å, and the spectral resolution in these ranges are (with both CCDs) $R \simeq 13\,000$, 15 000, and 18 000, respectively. These regions were chosen to cover several specific emission features expected from the environments of YHG: H α , [O I] $\lambda\lambda$ 6300, 6364 Å, [Ca II] $\lambda\lambda$ 7291, 7324 Å, and the Ca II $\lambda\lambda$ 8498, 8542, 8662 Å infrared triplet. Moreover, these regions cover many Fe I and Fe II lines with different excitation potentials, the hydrogen Paschen lines Pa(12)–Pa(18), as well as numerous other metal lines of different excitation

Table 2. Observation log of the echelle spectra

Date	JD (d)	Range (Å)	Inst.
2010-09-24	2455464	5216–6690	NES
2011-01-13	2455574	5208–6683	NES
2011-09-14	2455819	3985–6980	NES
2012-11-22	2456254	3770–9000	HERMES
2013-02-02	2456326	3916–6980	NES
2013-10-31	2456597	3770–9000	HERMES
2014-10-01	2456931	5417–8479	NES
2014-10-04	2456935	3770–9000	HERMES

and ionization states suitable for detailed studies of the atmospheric motions of the star. The log of the observations is given in Table 1.

For wavelength calibration, a comparison spectrum of a ThAr lamp was taken immediately after each exposure. The stability of the wavelength scale was verified by measuring the wavelength centroids of [O I] sky lines. The velocity scale remained stable within 1 km s^{-1} .

All data were reduced and heliocentric velocity corrected using standard IRAF² tasks. We also observed once per night a rapidly rotating star (HR 7880, Regulus, ζ Aql) as a telluric standard to perform the telluric correction.

Our data are supplemented by five spectra obtained with the high-resolution ($R \sim 60\,000$) Nasmyth Echelle Spectrograph (NES, see Panchuk et al. 2017) attached to the 6-m telescope at the Special Astrophysical Observatory (SAO) in Russia. The observations spread from 2010 September 24 to 2014 October 4. Details on the spectrograph and on the reduction procedure are provided by Klochkova et al. (2014).

Three high-resolution spectra ($R=85\,000$; Raskin et al. 2011) were obtained using the High Efficiency and Resolution Mercator Echelle Spectrograph (HERMES) mounted on the Mercator 1.2-m telescope at the Roche de los Muchachos Observatory, La Palma, Spain. The HERMES spectra were observed on 2012 November 22, 2013 October 31, and 2014 October 4. They have been calibrated with latest version of the HERMES pipeline for the typical echelle calibration steps of wavelength calibration, order-extraction, flat-fielding, background subtraction, and order merging. The quality of the echelle dispersion solutions was tested with the position of sharp telluric lines to check the wavelength scales are accurate. The spectra of October 2013 and 2014 consist of two subsequent exposures that were co-added for increasing the signal-to-noise ratios. The resulting flux spectra were normalized to the continuum flux level around selected spectral lines and in some spectral regions of interest.

The log of the echelle observations is given in Table 2.

All spectra were finally corrected for the systemic velocity of ρ Cas and normalized to the continuum. For the systemic velocity we adopted a value of -47 km s^{-1} , as was previously found by Lobel et al. (2003), Klochkova et al. (2014), and Klochkova et al. (2018).

² IRAF is distributed by the National Optical Astronomy Observatories, which are operated by the Association of Universities for Research in Astronomy, Inc., under cooperative agreement with the National Science Foundation.

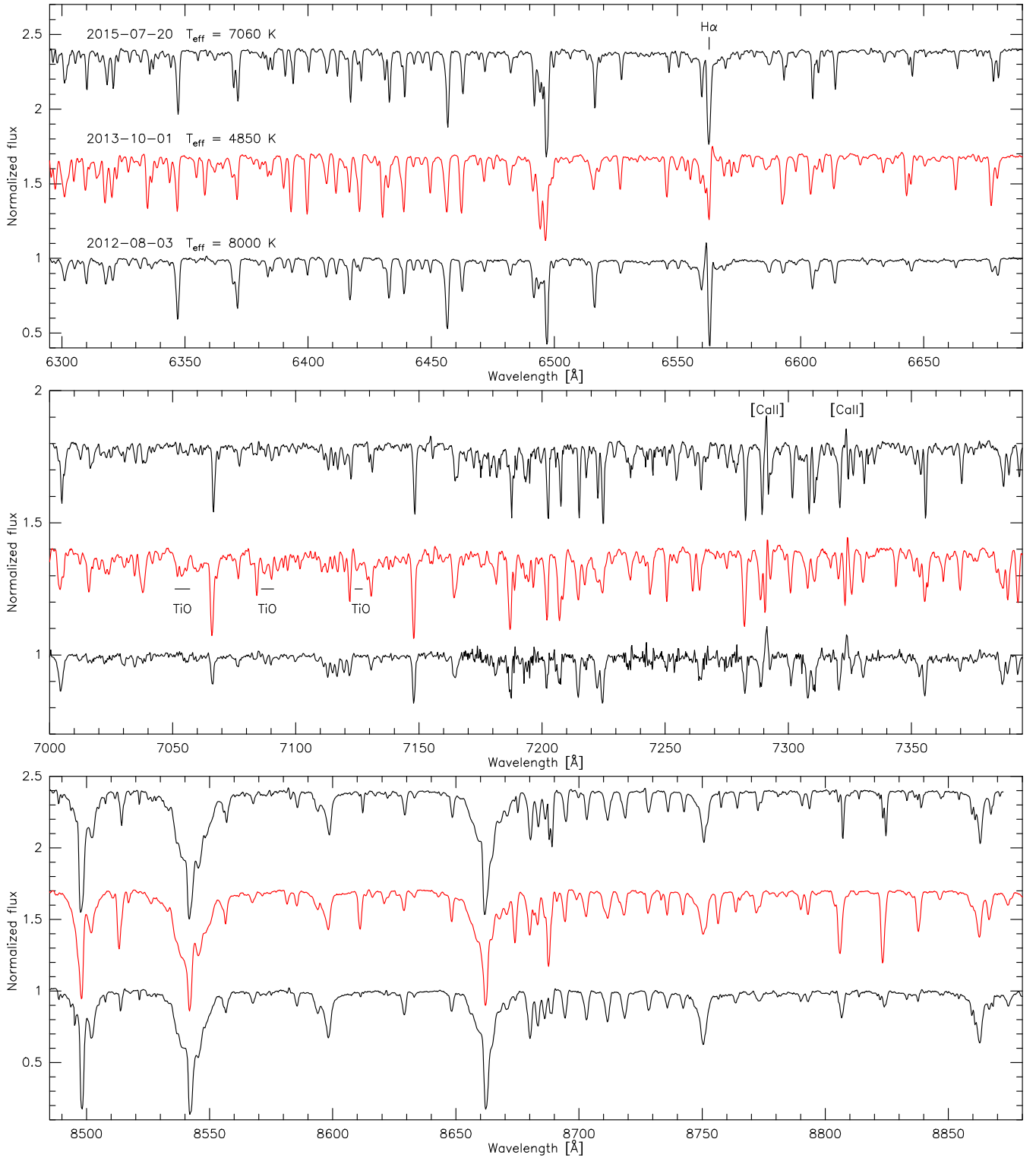


Figure 1. Ondřejov spectra during the hottest (bottom spectrum), outburst (coolest, middle spectrum) and recovered (top spectrum) phases in three different spectral regions. Prominent emission is seen in $\text{H}\alpha$ and in $[\text{Ca II}] \lambda\lambda 7291, 7324$. During outburst, weak TiO absorption appears. The positions and widths of the band heads are indicated. For best visualization the spectra in each wavelength region are offset arbitrarily.

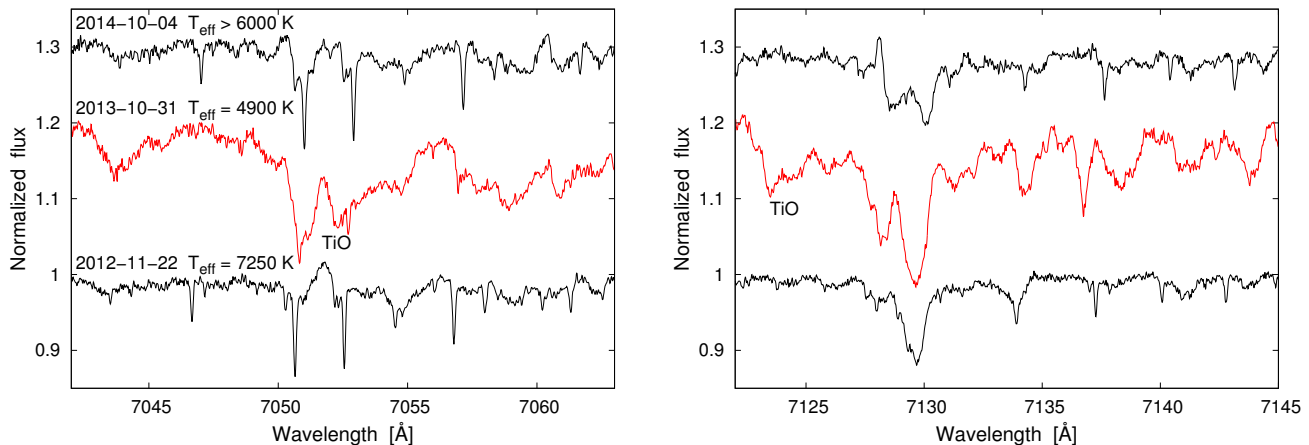


Figure 2. Clear presence of TiO bands in the HERMES data during the outburst in October 2013 compared to observations taken prior and later.

4 RESULTS

Our data collection spreads over about 4.5 years. The most prominent emission features in the spectra are $H\alpha$, in which we observe gradual changes in its blue and/or red emission wings, and the persistent, though weak emission in the $[\text{CaII}] \lambda\lambda 7291, 7324 \text{ \AA}$ lines. None of our spectra displays indication for $[\text{OI}] \lambda\lambda 6300 \text{ \AA}$ emission, in contrast to the hotter YHG counterparts IRC +10 420 or V509 Cas in which prominent emission in both sets of forbidden lines is usually seen (e.g., Aret et al. 2017a).

During the first half of our monitoring period we observe long-term line-profile variability in both the radial velocity and the shape of all lines. Such spectral variabilities for the atmospheric dynamics of ρ Cas in quiescence have been reported by many investigators (see Lobel et al. 2003; Gorlova et al. 2006; Klochkova et al. 2014, for comprehensive overviews) and generally comply with the interpretation of a combination of slow radial and non-radial pulsations on time-scales of several hundred days (e.g., Hassenstein 1934; Sheffer & Lambert 1986; Zsoldos & Percy 1991; Lobel et al. 1998; Percy et al. 2000).

In the following, we focus mainly on the second half of our observing epoch which is dominated by the new outburst. We present the various indications for the outburst and describe the post-outburst phase. We discuss the observed spectral features in connection and comparison with the reported dynamical characteristics of ρ Cas in the past. For illustration purposes, we present the full time-evolution of several selected lines in Figs. A1–A4 of the Appendix.

4.1 New outburst in 2013

In 2013 the spectroscopic behaviour of ρ Cas changed noticeably. In June, the cores of the lines of neutral elements such as FeI and TiI as well as the low- to intermediate-excitation lines of singly ionized elements appear strongly blue-shifted and additionally display a high-velocity blue-shifted wing (Figs. A1 and A2). In October, all these lines display deep blue-shifted absorption, while at the same time the lines of medium and high-excitation of ionized elements like FeII

and SiIII weaken and many previously not seen low excitation lines of neutral metals appear. This significant change in spectral appearance is demonstrated in Figure 1 where we show three spectra taken in the years 2012, 2013, and 2015 in the three covered wavelength regions. This drastic change in the strengths of the lines and the appearance of many additional low excitation lines of neutral metals indicate that during fall 2013 the atmosphere of ρ Cas resembled that of a considerably later spectral type.

Support for such an interpretation comes from the appearance of TiO absorption bands in the red spectral region in October 2013. This can be seen from inspection of the spectra shown in the middle panel of Fig. 1. For better visualization, the positions and widths of the TiO band heads are indicated by horizontal bars. These bands are also seen in the high-resolution spectra taken 30 days later with HERMES (Figure 2), confirming their identification in the lower resolution Ondřejov data. No TiO bands were seen in the spectra taken before or after.

The appearance of TiO bands together with the changes in the strengths and profile shapes of the photospheric lines listed above are clear signs for a (much) cooler atmosphere during this epoch. So far, these spectral characteristics were seen in ρ Cas only during its outbursts in the years 1946–47 (Popper 1947; Thackeray 1948), 1986 (Boyarchuk et al. 1988b), and the millenium outburst 2000–01 (Lobel et al. 2003), indicating that during 2013 ρ Cas underwent another outburst.

All previous outbursts of ρ Cas were connected with a significant drop in the light curve. To check the brightness behaviour during our spectroscopic observing campaign from July 2010 until the end of 2015, we constructed the light curve of ρ Cas based on V -band magnitudes retrieved from the AAVSO³ database. For a coherent set of data, we use only the light curve measurements obtained by Wolfgang Vollmann⁴, and complement them with data from the AAVSO Bright Star Monitor database. All values have been transformed to standard Johnson V magnitudes. To account

³ <https://www.aavso.org/>

⁴ <https://bav-astro.eu/rb/rb2015-1/23.pdf>

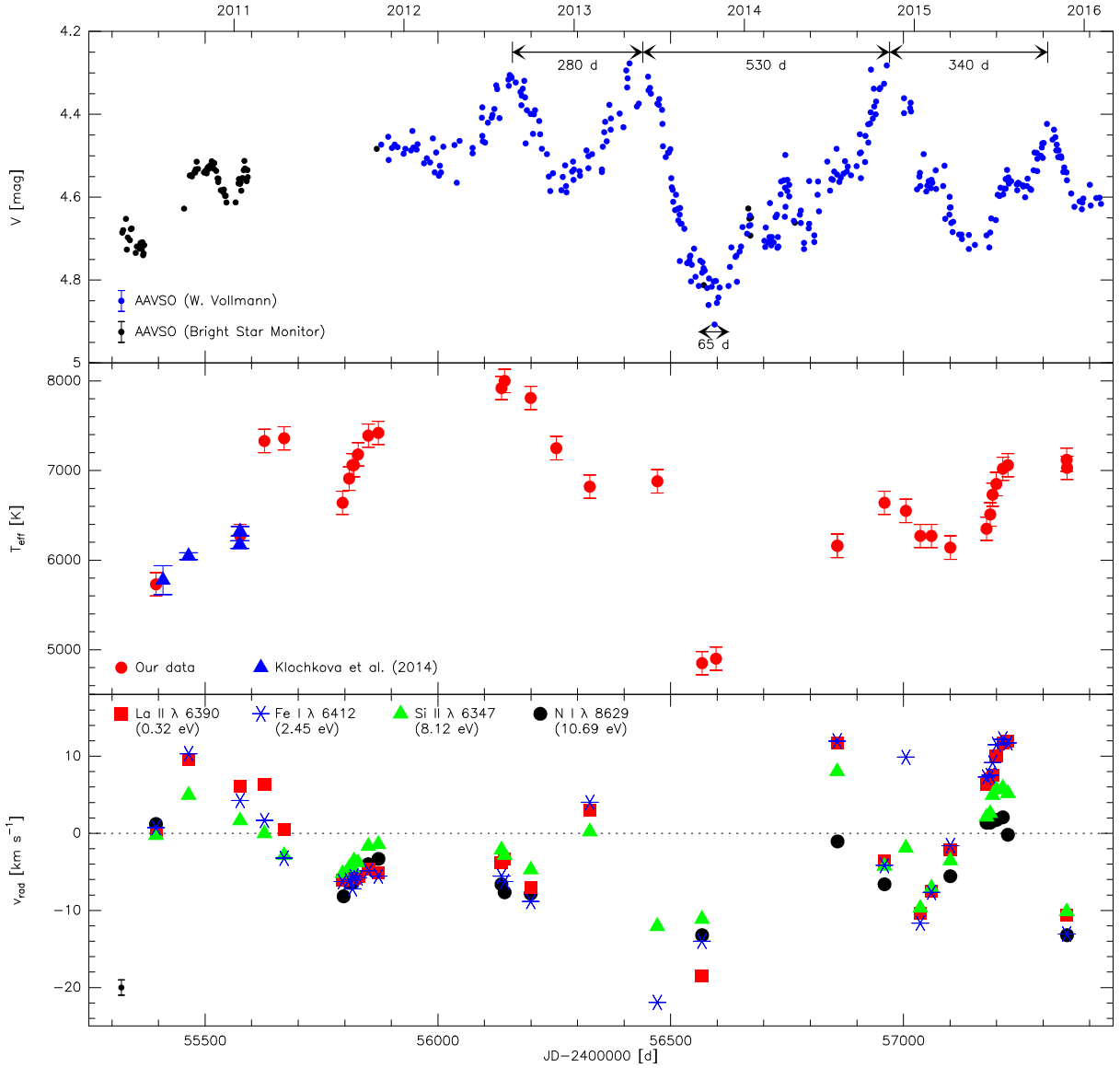


Figure 3. Top: V -band light curve of ρ Cas. Middle: Effective temperature variation derived from the Fe I λ 6431/Fe II λ 6433 line depth ratio. Bottom: Radial velocity variations in selected photospheric lines. Typical errorbars are indicated in each panel.

for small differences in the used filters, we shifted the values from Vollmann by +0.1 mag to match them to the data of the Bright Star Monitor. The combined V -band light curve is shown in the top panel of Figure 3. Typical errorbars range from 0.02 to 0.03 mag as indicated in the lower left corner.

The light curve displays three phases of maximum brightness of about 4.3 mag that were reached in August 2012, May 2013, and November 2014, and an additional one in October 2015, which was ~ 0.15 mag dimmer. The time spans between consecutive maxima are with approximately 280 d, 530 d, and 340 d rather irregular, however, they comply with former determinations of photometric periods of 280–300 d Zsoldos & Percy (1991) and Percy et al. (2000), and of a radial velocity periodicity of 520 d (e.g., Sheffer & Lambert 1986).

We also note the sudden drop in brightness by 0.55 mag in the year 2013 between end of May, when the star was still

at maximum brightness, and mid October, exactly at the time when we observe the presence of TiO bands in our red spectra. This pronounced minimum lasted for about 65 d. After that, the star started its recovery during which the brightness increased much shallower than it declined. The full recovery up to the next maximum took about a year. It is worth mentioning that the V brightness minimum in fall 2013 did not decrease to below the 5th magnitude, which is unlike the three previous outbursts recorded for ρ Cas where the star became much dimmer ($V > 5.0$ mag)

4.2 Temperature variation

The drop in brightness and the change in spectral appearance during the outburst are clear signs for a decrease in effective temperature of the star.

In the spectra of cool supergiants the lines of Fe I and

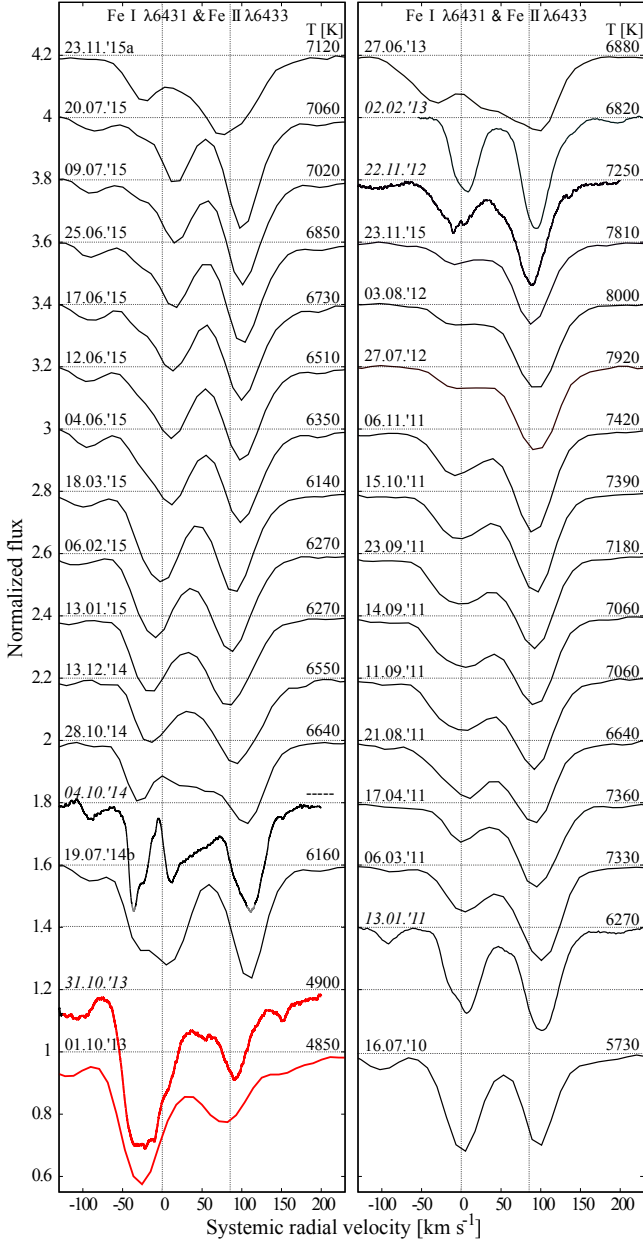


Figure 4. Line profile variation of Fe I λ 6431 and Fe II λ 6433 with their central positions indicated by the vertical lines. Spectra in red mark the outburst period. Dates listed in italic refer to high-resolution echelle spectra. The temperature value obtained from each observation is indicated.

Fe II have been found to be valuable temperature tracers, because their line strengths change in opposite directions for small variations in effective temperature. We utilize this property and estimate the temporal temperature variation of ρ Cas over the full observing period using the Fe I λ 6431/Fe II λ 6433 line depth ratio, calibrated by high resolution spectra (Elodie and UVES POP) of 19 late-A to early-K supergiants with precise T_{eff} values from the literature (Kovtyukh 2007). These data were supplemented with two hotter A-type stars with effective temperatures according to their spectral class (Currie et al. 2010). This

Table 3. Effective temperatures. Errors are ± 130 K.

Date	JD (d)	T_{eff} (K)	Note
2010-07-16	5394.5	5730	
2010-09-24	5464.4	—	(1)
2011-01-13	5574.6	6270	
2011-03-06	5627.2	7330	
2011-04-17	5669.6	7360	
2011-08-21	5795.4	6640	
2011-09-04	5809.4	6910	
2011-09-11	5816.4	7060	
2011-09-14	5819.6	7060	
2011-09-14	5819.4	—	(1)
2011-09-23	5828.5	7180	
2011-10-15	5850.5	7390	
2011-11-06	5872.2	7420	
2012-07-27	6136.6	7920	
2012-08-03	6143.4	8000	
2012-09-28	6199.4	7810	
2012-11-22	6254.4	7250	
2013-02-02	6326.3	6820	
2013-06-27	6471.5	6880	
2013-10-01	6567.4	4850	
2013-10-31	6597.4	4900	
2014-07-18	6857.6	6160	
2014-07-19	6858.5	6160	
2014-10-01	6931.6	—	(1)
2014-10-04	6935.4	—	(2)
2014-10-28	6959.3	6640	
2014-12-13	7005.3	6550	
2015-01-13	7036.2	6270	
2015-02-06	7060.2	6270	
2015-03-18	7100.6	6140	
2015-06-04	7178.5	6350	
2015-06-12	7186.5	6510	
2015-06-17	7191.4	6730	
2015-06-25	7199.6	6850	
2015-07-09	7213.5	7020	
2015-07-20	7224.4	7060	
2015-11-23	7350.5	7120	
2015-11-24	7351.4	7030	

(1) SAO spectrum with gap at 6430 Å.
(2) Strong emission in Fe I λ 6430.

calibration provides temperature estimates with an error of ± 130 K. The profiles of the two adjacent lines are shown in Figure 4, and the temperature values obtained from our medium- and high-resolution observations are given in Table 3. For certain epochs no temperature could be derived due to gaps in the echelle spectra of NES or during the phase when the profiles display strong pollution with a pronounced emission component, as observed for example on 2014 October 4. The temperature variation is shown in the middle panel of Figure 3.

As Klochkova et al. (2014) have also observed ρ Cas back in 2010–2011 and determined effective temperatures from their high-resolution spectra, we superimpose their values on our temperature curve (blue dots in the middle panel of Figure 3) and find that our determinations from lower spectral resolution data agree very well with theirs so that we are confident about our temperature measurements.

In general, the observed variations in effective temper-

ature follow the trend of the light curve, as was also noted by Lobel et al. (2003): the star appears hotter during bright phases and cooler during fainter phases and during the outburst. However, we note that there are epochs in which the correlation between temperature and brightness is less accurate. These are the epochs during the onset of the outburst (June 2013) and in the recovery phase (July – October 2014). Here, the absorption lines are strongly distorted due to the increased kinematics within the rapidly expanding atmosphere and due to the appearance of superimposed emission. Therefore, we would like to caution that the method of the line depth ratio has its limitations. It can provide only reliable temperature values as long as none of the absorption lines is saturated or filled/polluted with a significant amount of emission. Moreover, we would like to stress that in an object like ρ Cas with a very extended, hence diluted, and highly dynamical atmosphere, the variation in brightness is not solely caused by the variation in effective temperature. The global dynamics within the atmosphere of a pulsating star can severely influence the optical depth, i.e., the apparent radius of the star, and consequently impact the brightness as well. It is therefore not surprising that our temperature estimates during the outburst imply an equally cool temperature for ρ Cas as during the millenium outburst, which is verified by the appearance of TiO band absorption, although the V brightness dropped by only half the value.

4.3 Atmospheric dynamics

The outburst is expected to be accompanied by an enhanced atmospheric dynamics. In stars with very extended atmospheres such as ρ Cas the formation of individual spectral lines is determined by the contribution function reaching maxima in different regions of the atmosphere. The locations of these maxima depend on the excitation energies of the individual lines. Hence, lines with diverse excitation energies can yield different radial velocity values, because the contributions to their emergent profiles can originate from various portions along the atmospheric height. These formation regions are typically associated with different velocities within a pulsating atmosphere.

To study the vertical velocity structure within the extended, pulsating photosphere of ρ Cas, we selected several strategic absorption lines of different elements in various ionization stages and covering a large range in excitation energies. We measured the midpoint positions of the full line width at half maximum and computed from it the center-of-gravity radial velocity of each absorption line associated with the mean line formation region. This method minimizes the influence of the wind, which manifests itself in the profiles by extended blue wings. Our measurements are shown for four representative lines in the bottom panel of Figure 3. Typical sources for errors result from the stability of the spectrograph and from the adjustment of the continuum. We estimate that the total error in velocity will not exceed $\pm 1 \text{ km s}^{-1}$. This errorbar is included in the bottom left of the plot.

In general, we observe that all lines display radial velocity variations. The low-excitation lines of La II $\lambda 6390$ and Fe I $\lambda 6412$ with excitation energies of 0.3 eV and 2.5 eV, respectively, are most sensitive to conditions in the uppermost layers of the photosphere. During pre-outburst (i.e. quies-

cence) phase, these lines have usually the highest amplitudes with total values of $15\text{--}17 \text{ km s}^{-1}$. The two high-excitation lines, Si II $\lambda 6347$ (8.12 eV) and N I $\lambda 8629$ (10.69 eV), trace the kinematics within the deeper photosphere, and their amplitude is with about $9\text{--}10 \text{ km s}^{-1}$ slightly lower. We note, however, that our observing cadence is rather coarse so that these amplitudes can only be considered as rough estimates and consequently present lower limits to the real kinematics during quiescence. In fact, much tighter sampling resulted in slightly higher amplitude values (e.g., Sheffer & Lambert 1986; Lobel et al. 1998, 2003; Klochkova et al. 2014) but maintaining the general trend of higher amplitudes with lower excitation energy.

Immediately before, during and after the outburst the amplitudes of all lines are greatly enhanced. Particularly interesting is the strong blueshift and the formation of an additional high-velocity blue wing in the low-excitation lines in June 2013 (see Fig. A1) reaching out to about -110 km s^{-1} , hence indicating that rapid expansion of the outermost layer has started already when the brightness was still close to maximum. Such a phase lag between brightness and radial velocity was also found by Lobel et al. (2003).

The high radial velocity amplitudes observed more than one year after the outburst (i.e., after the recovery of the brightness, see also the recent work by Klochkova et al. 2018) might indicate that the atmosphere itself did not yet fully settle back to its equilibrium, i.e., quiescence state but is still strongly oscillating. Support for such an interpretation is provided by the high-excitation lines forming generally much deeper in the atmosphere. These lines also show large velocity displacements (see Figs. A2 and A3), in agreement with a highly dynamical and disordered photosphere.

4.4 Emission lines

Another noteworthy detected property is the emergence of emission lines, and most interesting is hereby the emission in the line Fe I $\lambda 6359$. It is observed in our post-outburst spectra in 2014 as well as during phases of maximum brightness epochs within the quiescence phase of ρ Cas (Fig. A5). Fe I $\lambda 6359$ belongs to the ‘splitting sensitive’ group of lines (see Sargent 1961; Lobel et al. 1998, 2003; Klochkova et al. 2014, for the discovery and definition of line splitting in the spectrum of ρ Cas) based on its low excitation potential (0.86 eV).

In contrast to this occasional appearance of emission, Lobel et al. (1998) and Gorlova et al. (2006) noted that an emission component in the forbidden line [Ca II] $\lambda 7324$ is always present. As this line appeared to be static and hence circumstellar in origin, its position in the spectra at -47 km s^{-1} has been used to determine the systemic radial velocity of ρ Cas.

The forbidden lines of [Ca II] $\lambda \lambda 7291, 7324$ are also seen in our red spectra (middle panel of Fig. 1). Inspection of our time series reveals that the shape and strength of their profiles strongly depends on the interplay between the static emission and the underlying dynamic (in position, shape and strength) absorption profile (Fig. A5). In particular in the first half of 2015 the emission is basically completely compensated by deep and broad underlying absorption components.

Examination of the position of the emission compo-

nent in the Fe I $\lambda 6359$ line in comparison to [Ca II] $\lambda 7324$ shows that a tight correlation exists in the behaviour of both lines. This is demonstrated over the full time series shown in Fig. A5 and highlighted in Fig. 5 where we display the profiles of [Ca II] $\lambda 7324$ and Fe I $\lambda 6359$ in four selected epochs (from top to bottom): the most blue-shifted, the most red-shifted, and two intermediate ones. Obviously, the emission bumps in Fe I $\lambda 6359$ are in phase with those of [Ca II] $\lambda 7324$. Therefore, we conclude that the profile of Fe I $\lambda 6359$ also contains a static circumstellar emission component, exactly as it is the case for [Ca II]. This static emission component disturbs the absorption profile and results in a permanent ‘splitting’ of the line, although it is not always prominent or obvious in the profiles.

Sargent (1961) has found that splitting occurs in lines with an excitation potential up to 2.9 eV of their lower levels. Many of these potentially split lines actually behave similarly to Fe I $\lambda 6359$. Depending on their strength and sensitivity to temperature changes, they exhibit the splitting only at certain epochs. For instance, several absorption lines of Fe I in our spectral time series are split at just one epoch (2014-10-04) while during the remaining observation period they display pure absorption profiles albeit varying with moderate asymmetry. Also for these lines, we can recognize that the asymmetry within the line profiles can be ascribed to a static circumstellar emission component in line (and in phase) with the emission of [Ca II] $\lambda 7324$. Likewise we might interpret the asymmetries seen in Fe I lines with excitation potentials higher than 2.9 eV with circumstellar emission (see Fe I $\lambda 6400$ with EP = 3.60 eV in Fig. A1) because they all follow the same trend as the Fe I $\lambda 6359$ line.

When inspecting lines with much higher excitation potential (see, e.g., Si II $\lambda 6347$ with EP = 8.12 eV and Ni I $\lambda 8629$ with EP = 10.69 eV in Fig. A2 and Fig. A3, respectively) their absorption profiles display no obvious indication for superimposed circumstellar emission. For demonstration purposes we included the profile of Ni I $\lambda 8629$ in Fig. 5. In contrast to the low-excitation lines that are contaminated with circumstellar emission, this high-excitation line displays radial velocity shifts around the systemic velocity together with a mild wiggling of its profile shape, in agreement with pulsation movements in the atmosphere of ρ Cas.

Finally, it should be mentioned that H α exhibits time variable emission components in both line wings (Fig. A4). This was also noted by Gorlova et al. (2006). However, we want to stress that the emission variability seen in H α is not in phase with [Ca II] $\lambda 7324$, rendering it less likely that this emission is of static circumstellar origin. Instead, H α forms over a large volume of the stellar photosphere extending into the base of the wind where the conditions in terms of density and temperature are still favourable to partially ionize hydrogen and to generate recombination line emission in a measurable amount.

5 DISCUSSION

5.1 Circumstellar material

In general, emission lines of [Ca II] are a reasonable tracer for dense, circumstellar gas around hot (e.g., Kraus et al. 2010; Aret et al. 2012; Maravelias et al. 2018) and cool

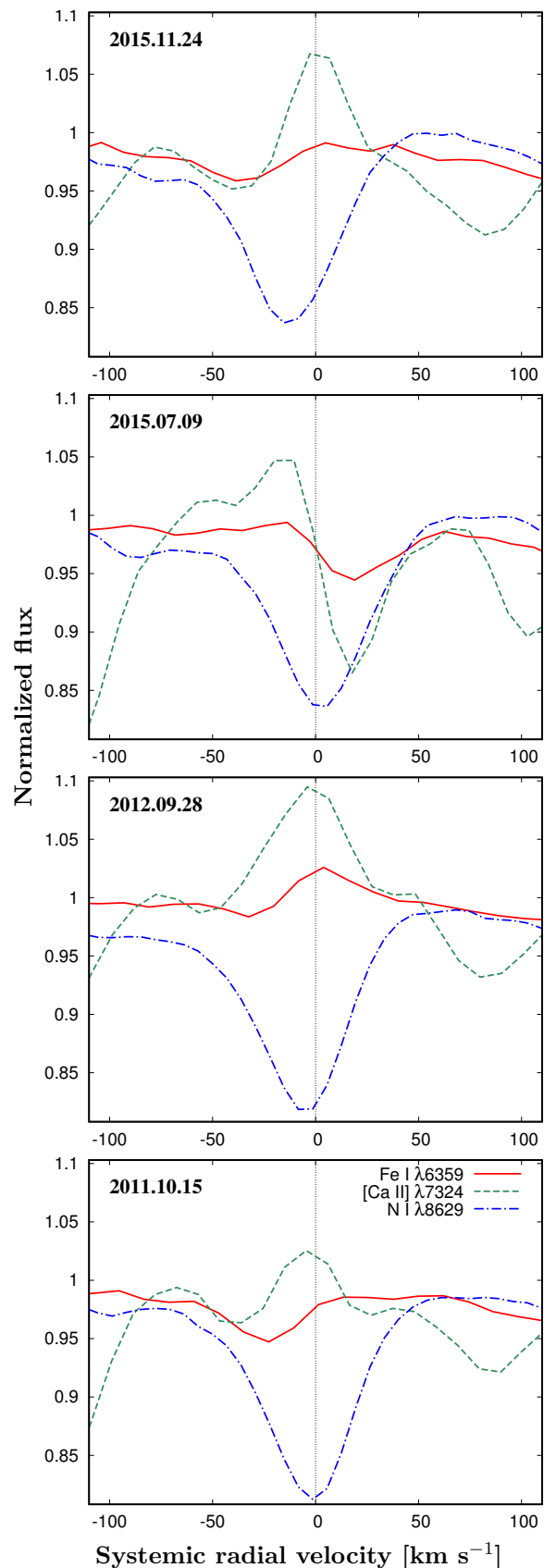


Figure 5. Comparison of line profiles in four selected epochs. The emission component in Fe I $\lambda 6359$ varies synchronously with [Ca II] $\lambda 7324$ implying static emission in the low-excitation iron line, which is not seen in the high-excitation Ni I $\lambda 8629$ line.

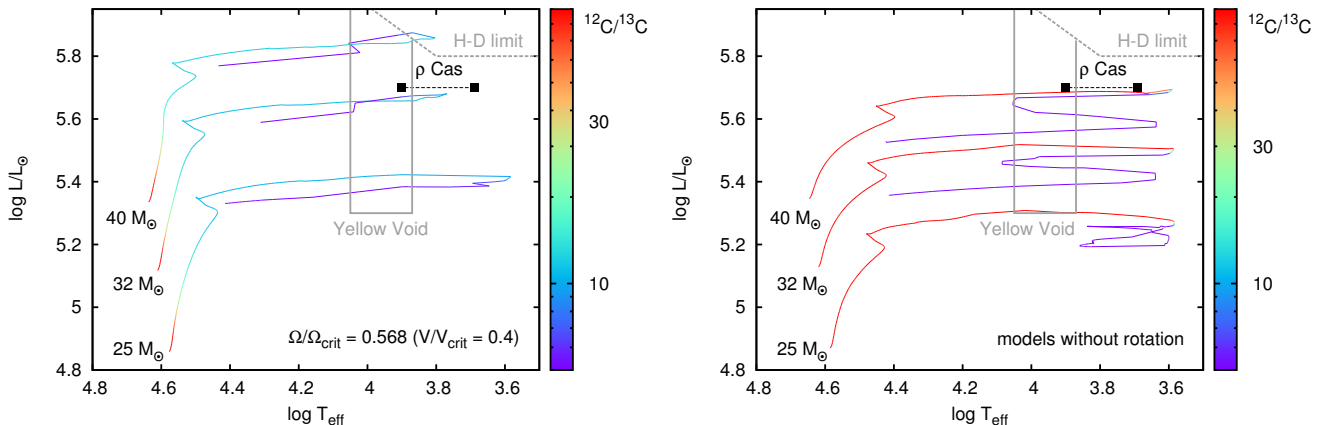


Figure 6. Position of ρ Cas in the HR diagram along with Geneva stellar evolutionary tracks for solar metallicity models with (left panel) and without (right panel) rotation (from Ekström et al. 2012). The luminosity of ρ Cas is from Humphreys (1978). The temperature spreads from the hot, quiescent to the cool, outburst state (Table 3). The positions of the Yellow Void instability region (de Jager & Nieuwenhuijzen 1997) and the Humphreys-Davidson limit (Humphreys & Davidson 1994) are shown in gray. The color coding (in logarithmic scale) refers to the surface abundance ratio of $^{12}\text{C}/^{13}\text{C}$.

stars (Humphreys et al. 2013, 2017; Aret et al. 2017a,b). Our findings of static circumstellar emission in basically all low to medium-excitation lines in the spectra of ρ Cas with the same spectroscopic appearance as the [CaII] lines hence reinforces, that the star must be surrounded by a significant amount of gas, possibly confined in a stable shell or ring.

Further support for warm and dense circumstellar material is provided by molecular emission, primarily by CO band emission. These bands have been detected in the near-infrared spectra ($> 2.3 \mu\text{m}$) of many B[e] supergiants, in which the emission typically originates from a circumstellar ring or the inner edge of a molecular disc (Kraus et al. 2000, 2016, 2017; Liermann et al. 2010, 2014; Cidale et al. 2012; Wheelwright et al. 2012; Oksala et al. 2012, 2013; Muratore et al. 2015; Torres et al. 2018; Maravelias et al. 2018). In ρ Cas, CO band emission was first reported by Lambert, Hinkle & Hall (1981). The excitation of these bands requires a temperature range of 2000–5000 K which is much lower than the stellar effective temperature. Monitoring of the CO bands revealed that they switch from pure emission to pure absorption and back (Gorlova et al. 2006; Yamamuro et al. 2007). Interestingly, the phases of pure and intense emission were found to coincide with phases of atomic line emission, which agree with phases of maximum light.

According to Gorlova et al. (2006) the CO band emission is centred on the systemic velocity and displays only mild radial velocity variations, whereas the absorption can appear significantly red or blue-shifted (up to 30 km s^{-1}). Based on these findings we propose that the CO band emission itself is always present in the spectra, just as the [CaII] emission, and likewise originates from the circumstellar gas, while the absorption forms in the outermost atmospheric layer.

Considering that during the atmospheric expansion caused by the pulsation activity of the hypergiant star the temperature within its very outer layer can be considerably lower than the effective temperature, and hence also lower than the dissociation temperature of CO which is around

5000 K, the conditions for the formation of CO molecules can be met. These hot molecules will absorb the continuum emission from the star in the near-infrared, causing CO band absorption. With further expansion hence cooling, the absorption bands superimposing the circumstellar emission will first compensate the emission and then continue to grow and dominate the near-infrared spectral appearance until the expansion stops and contraction sets in, reversing the process. During phases of maximum light the star is hottest and therefore most compact. Even its outermost layers are too hot for CO molecules to exist. Therefore, no absorption takes place and only the circumstellar emission is observable.

The line profiles of the circumstellar emission components are very narrow and hence do not provide information about the dynamics within their formation region. For instance, the profiles of the [CaII] lines, which in our spectra are narrow and single-peaked, display no indication for kinematical broadening beyond our spectral resolution. The same holds for the stable circumstellar emission component of the Fe I $\lambda 5328$ line measured by de Jager (1998) in their high-resolution spectra. If ρ Cas is surrounded by a Keplerian rotating ring (or disc), as was proposed to be the case for the two hotter YHGs IRC +10420 (Davies et al. 2007) and V509 Cas (Aret et al. 2017b), the orientation of the ρ Cas system would have to be (close to) pole-on.

So far, the origin of the static circumstellar gas is unclear. It might be the remnant of one of the previous mass ejection, i.e. outburst events, or even of a possible previous RSG mass-loss. de Jager (1998) proposed that the material confinement could be caused by a stationary shock at the interface of the interstellar medium and the stellar wind. In this scenario, the stellar wind streams with high velocity into the shock and leaves it with very low velocity, explaining the stable position of the emission and the narrowness of the lines (see Chap. 4, p. 43 in Lobel 1997). Alternatively, depending on the pressure of the interstellar medium, the interface between the stellar wind and the interstellar medium

might take the form of a stagnation region determined by a stagnation point, which is known as the classical scenario of an astrosphere (e.g., Nickeler et al. 2006, 2014). Along the stagnation line (passing through the stagnation point) and all other streamlines in its vicinity, the speed of the matter reduces to (almost) zero velocity on both sides in the stagnation region, implying an extremely long arrival time for the material from the star.

In any case, abundance studies of the circumstellar matter in relation with a closer look at the evolutionary state of ρ Cas might help to discriminate between the various scenarios.

5.2 Evolutionary state of ρ Cas

Boyarchuk et al. (1988a) reported a large sodium overabundance from a non-LTE analysis of optical Na I lines. They measured $[\text{Na}/\text{H}]=0.72$ and $[\text{Na}/\text{Fe}]=0.67$ (their Table 3). The latter value is the largest value for the F-type supergiants they analysed, signaling an excess abundance of sodium in this Yellow Hypergiant. Alike, the intense emission in NaI detected in the near-infrared spectra (Gorlova et al. 2006; Yamamuro et al. 2007) has been assigned to a high NaI abundance (Takeda & Takada-Hidai 1994; El Eid & Champagne 1995). Moreover, Boyarchuk & Boyarchuk (1981) and Boyarchuk & Lyubimkov (1983) derived a carbon abundance of $12+\log(\text{C}/\text{H}) = 8.06$ and 8.03 , respectively, based on measurements of the line equivalent widths of six representative carbon lines in the optical spectra of ρ Cas. Based on these sodium abundance measurements, de Jager (1998) proposed that ρ Cas must be a post-red supergiant, evolving along the blueward loop in the HR-diagram.

Additional information about the possible evolutionary state of ρ Cas is provided by the carbon isotope ratio $^{12}\text{C}/^{13}\text{C}$. While this ratio cannot be directly measured on the stellar surface, Kraus (2009) argued that it translates into the molecular isotope abundance ratio $^{12}\text{CO}/^{13}\text{CO}$ which can be easily derived from even moderate-resolution near-infrared spectra. The $^{12}\text{CO}/^{13}\text{CO}$ ratio measured within the circumstellar material hence traces the surface $^{12}\text{C}/^{13}\text{C}$ ratio at the time of mass ejection. Based on the strength of the ^{13}CO emission and absorption features seen in their high-resolution near-infrared spectra Lambert et al. (1981) derived a carbon isotope ratio of $^{12}\text{C}/^{13}\text{C} = 30$.

Using the Geneva stellar evolutionary tracks from Ekström et al. (2012) for significantly rotating ($\Omega/\Omega_{\text{crit}} = 0.568$, corresponding to $V/V_{\text{crit}} = 0.4$) and non-rotating stars with solar metallicity, we compute the carbon isotope ratio along the tracks. The results are shown in Fig. 6. The position of ρ Cas is included in both plots. The stellar luminosity is taken from Humphreys (1978), and the minimum (during outburst) and maximum temperature values follow from our analysis (Table 3). In the models with significant stellar rotation a carbon isotope ratio of 30 is reached already during the main-sequence evolution, whereas in the temperature range of ρ Cas the ratio is about 10.5 in the pre-RSG stage and drops to 6.65 in the post-RSG stage. Along the tracks with no rotation the stars keep the initial (interstellar) value of the carbon isotope ratio of ~ 90 from the main sequence up to the RSG stage. Only during the RSG phase, the ra-

tio quickly drops and reaches a post-RSG value of about 7 within the current temperature range of ρ Cas.

Considering these two extremes, there should also exist stellar models with moderate rotation in which the observed $^{12}\text{C}/^{13}\text{C}$ ratio of 30 could be reached during the pre-RSG phase. To search for such models, we utilized the interpolation interface provided by the Geneva group⁵. Using the database for solar metallicity, we retrieved tracks for the mass range 32 to $40 M_{\odot}$ in steps of $1 M_{\odot}$ and with rotation rates ($\Omega/\Omega_{\text{crit}}$) such that the carbon isotope ratio of 30 ± 1 is achieved in the post-main sequence but pre-RSG state. The required rotation rate decreases slightly for decreasing stellar mass. These models are shown in the left panel of Fig. 7. We furthermore used these models to compute the evolution of the carbon abundance on the stellar surface. The results are presented in the right panel of Fig. 7 together with ρ Cas and its measured value of $12+\log(\text{C}/\text{H}) = 8.03$ from Boyarchuk & Lyubimkov (1983). Assuming that the carbon abundance is representative of the surface abundance at the time of the ejection, and considering a conservative value of ± 0.1 as error to the carbon abundance value, the observed carbon deficiency cannot be achieved during the pre-RSG evolution if at the same time the $^{12}\text{C}/^{13}\text{C}$ ratio of 30 should be kept.

We also inspected model predictions for the evolution of the sodium surface abundance in these mass and rotation velocity bins. While sodium abundances are not provided by the Geneva group, the stellar evolution tracks of Brott et al. (2011) contain sodium surface abundances along the evolution from the main-sequence up to the RSG state for massive stars rotating with a diversity of rates. We inspected their models for initial masses of 30 , 35 , and $40 M_{\odot}$ and rotation speeds up to $V/V_{\text{crit}} \leq 0.4$. We found that these models provide a maximum achievable sodium enrichment of $[\text{Na}/\text{H}] < 0.3$ and $[\text{Na}/\text{Fe}] < 0.25$. These values are far below the observed ones in ρ Cas of 0.72 and 0.67 , respectively (Boyarchuk et al. 1988a).

Considering the evolution of a $40 M_{\odot}$ star without (or with only very mild) rotation, the observed abundances of carbon and its isotope (right panels of Figs. 7 and 6, respectively) as well as the overabundance of Na can be reached during or beyond the RSG evolution of the star. These abundance considerations suggest that ρ Cas would be in its post-RSG (or blue loop) evolutionary phase. In this scenario, the observed $^{12}\text{C}/^{13}\text{C}$ ratio of 30 would correspond to material that was released during a previous RSG stage.

Based on the velocity-luminosity relation for RSGs derived by Mauron & Josselin (2011), we obtain a wind velocity of $\sim 35 \text{ km s}^{-1}$ during the RSG state of ρ Cas. Considering that the enhanced mass loss within the RSG phase took place about $10\,000 \text{ yr}$ ago, the material would have travelled over a length of roughly 0.36 pc , which corresponds to an angular distance of $\sim 24''$ at the distance of 3.1 kpc for ρ Cas (Lobel et al. 2003). This angular distance is too small to be seen on, e.g., WISE images, on which ρ Cas is saturated. This distance is also much smaller than the size of a regular wind-blown bubble resulting from the previous blue supergiant phase, so that we can exclude that the material is located within the astrosphere or shock region with the interstellar medium. On the other hand, this distance is too

⁵ <https://www.unige.ch/sciences/astro/evolution/en/database/syclist/>

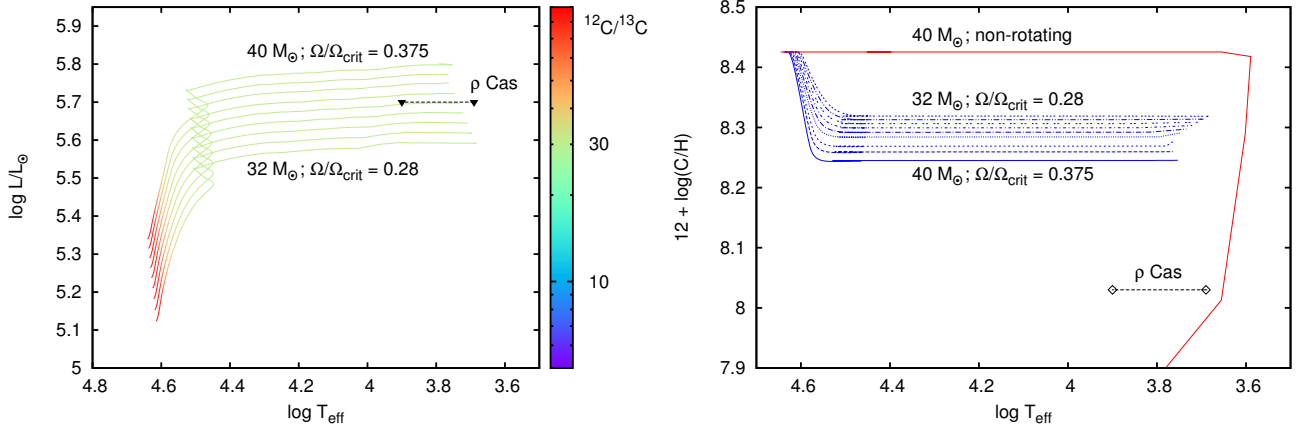


Figure 7. Left: Geneva stellar evolutionary tracks up to the RSG state for models between 32 and $40 M_{\odot}$ with rotation. The rotation rate is determined such that the star maintains a $^{12}\text{C}/^{13}\text{C}$ ratio of 30 from the end of the main-sequence up to the position of ρ Cas. Right: Evolution of the surface ^{12}C abundance for the same parts of the stellar evolution models as in the left panel. Included are the results for the $40 M_{\odot}$ model without rotation up to the blue loop and the measured value of $12 + \log(\text{C}/\text{H}) = 8.03$ of ρ Cas from [Boyarchuk & Lyubimkov \(1983\)](#). A conservative error estimate for this value is ± 0.1 .

large to be seen on the HST images presented by [Schuster et al. \(2006\)](#), and too large to guarantee that the material is dense and hot enough to produce measurable amounts of CO band emission. Therefore, we believe that the post-RSG wind, which is faster but much less massive, interacts with the material released during the RSG phase. This interaction can lead to a compression and heating of the old material (with the appropriate carbon isotope ratio) and hence give rise to the observed, static CO band emission. The temperature of the CO gas is much higher than the dust sublimation temperature. In the region of CO band emission, the physical parameters within the environment might hence prevent the efficient formation of dust, which could be another reason for the lack of a detectable dusty nebula around ρ Cas.

For its spectral type, and considering that ρ Cas is presumably a very slow rotator, it displays extremely broad absorption lines. These were suggested to be broadened by macroturbulence. This type of line broadening is typically found in early-type (OB) supergiants in which pulsations play a significant role together with stellar rotation (see, e.g., [Ryans et al. 2002](#); [Simón-Díaz et al. 2010](#); [Aerts et al. 2009](#); [Kraus et al. 2015](#)), and is one of the criteria to discriminate YHG from YSGs ([de Jager 1998](#)). While ρ Cas is known to pulsate, not much is known about its real rotation velocity, although [Lobel et al. \(1998\)](#) derived a value of $v \sin i \simeq 25 \text{ km s}^{-1}$ from line-profile fitting.

To investigate the possible contribution of rotation to the line profile broadening of ρ Cas, we analysed photospheric lines using the method of Fourier transformation. This method only works properly for symmetric profiles. However, symmetric line profile shapes are rather rare in our data of ρ Cas and basically only seen in two nights. Also, given the spectral resolution of our data, the Fourier transformation can recover only rotation velocities projected to the line-of-sight higher than $v \sin i \sim 15 \text{ km s}^{-1}$ with high confidence. The results from our analysis are shown in Fig. 8 for different elements within the same night (top panel) and for the same element in the two different nights (bottom

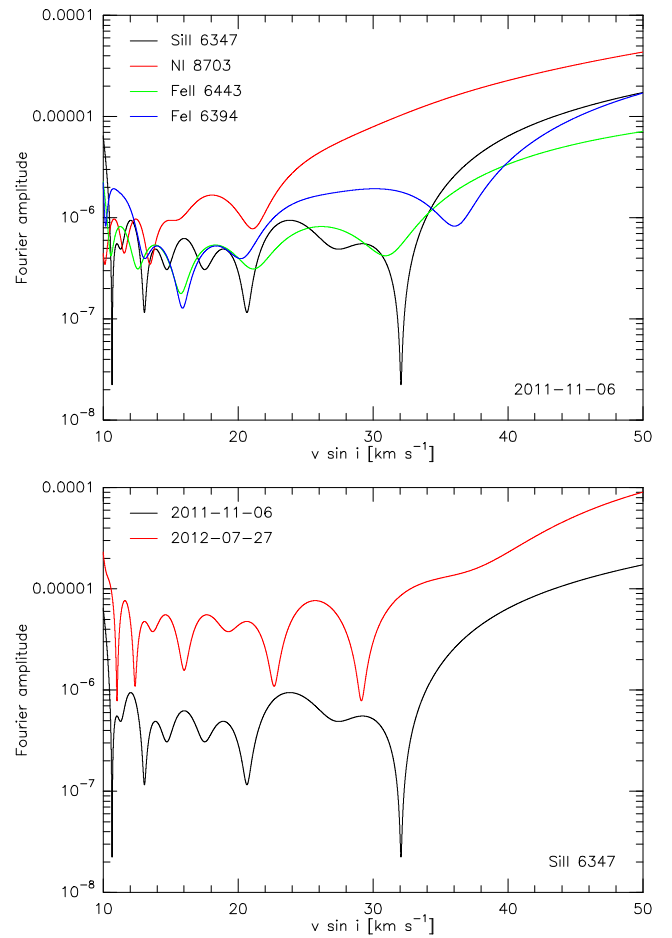


Figure 8. Results from the Fourier transformation of selected lines with apparently symmetric profile shapes. Top: different lines within the same night; bottom: same line within two different nights.

panel). If a rotation component projected to the line of sight higher than 15 km s^{-1} would be present in these profiles, the zero points of all elements should indicate the same value of $v \sin i$. However, our data provide no consistent value for the rotation velocity. Therefore, we conclude that the line broadening seen in ρ Cas is primarily (maybe even exclusively) due to the large-scale atmospheric dynamics controlled by pulsations.

6 CONCLUSIONS

Based on long-term photometric and spectroscopic monitoring of the YHG ρ Cas we found that it underwent a new outburst in 2013 with a temperature decrease of $\sim 3000 \text{ K}$ and a drop of $\sim 0.6 \text{ mag}$ in brightness. The large variability in radial velocities of basically all photospheric lines even after the recovery of the stellar brightness indicates that the atmosphere of ρ Cas is still far from being back in equilibrium.

Our data indicate that basically all low- to medium-excitation lines display a static emission component that displays the same behaviour as the circumstellar [CaII] emission lines. Consequently, we propose that the emission features seen especially during the hot, maximum light phases of ρ Cas are all circumstellar in nature, including the emission in CO bands. Based on an analysis of the $^{12}\text{C}/^{13}\text{C}$ abundance ratio, we further propose that this circumstellar material is the remnant from strongly enhanced mass-loss during the previous RSG state. This material is possibly compressed and heated by the subsequent post-RSG wind. But its distance from the star is too small to be visible on currently available infrared images due to saturation issues.

Follow-up monitoring of ρ Cas is indispensable to study in more detail the global dynamics of its atmosphere, to analyse its pulsation activity, and to identify new outburst phases, which will help the star to reach again stable atmospheric conditions on its way through the Yellow Void.

ACKNOWLEDGMENTS

We thank the technical staff at the Ondřejov Observatory for the support during the observations. This research made use of the NASA Astrophysics Data System (ADS) and of the SIMBAD database, operated at CDS, Strasbourg, France. MK, AA, and DHN acknowledge financial support from GA ČR (grant number 17-02337S). IK and TE acknowledge financial support from the institutional research funding IUT40-1 of the Estonian Ministry of Education and Research, and VGK from the Russian Foundation for Basic Research (grant 18-02-00029 a). The Astronomical Institute Ondřejov is supported by the project RVO:67985815. This research was also supported by the European Union European Regional Development Fund, Project “Benefits for Estonian Society from Space Research and Application” (KOMEET, 2014-2020.4.01.16-0029). We thank the referees for careful reading of our manuscript.

This work is based on observations collected with the Perek 2-m telescope at Ondřejov Observatory, Czech Republic, the 6-m telescope at the Special Astrophysical Observatory (SAO), Russia, and the Mercator 1.2-m telescope

on La Palma. We acknowledge with thanks the variable star observations from the AAVSO International Database contributed in particular by W. Vollmann.

REFERENCES

- Aerts C., Puls J., Godart M., Dupret M.-A., 2009, *A&A*, **508**, 409
- Aret A., Kraus M., Muratore M. F., Borges Fernandes M., 2012, *MNRAS*, **423**, 284
- Aret A., Kolka I., Kraus M., Maravelias G., 2017a, in Miroshnichenko A., Zharikov S., Korčáková D., Wolf M., eds, *Astronomical Society of the Pacific Conference Series Vol. 508, The B[e] Phenomenon: Forty Years of Studies*. p. 239 ([arXiv:1611.04490](https://arxiv.org/abs/1611.04490))
- Aret A., Kraus M., Kolka I., Maravelias G., 2017b, in Balega Y. Y., Kudryavtsev D. O., Romanyuk I. I., Yakunin I. A., eds, *Astronomical Society of the Pacific Conference Series Vol. 510, Stars: From Collapse to Collapse*. p. 162 ([arXiv:1611.06044](https://arxiv.org/abs/1611.06044))
- Beardsley W. R., 1961, *ApJS*, **5**, 381
- Boyarchuk A. A., Boyarchuk M. E., 1981, *Bulletin Crimean Astrophysical Observatory*, **63**, 68
- Boyarchuk A. A., Lyubimkov L. S., 1983, *Bulletin Crimean Astrophysical Observatory*, **66**, 119
- Boyarchuk A. A., Hubeny I., Kubat I., Lyubimkov L. S., Sakhbullin N. A., 1988a, *Astrophysics*, **28**, 202
- Boyarchuk A. A., Boyarchuk M. E., Petrov P. P., 1988b, *Tartu Astrofüüsika Observatoorium Teated*, **92**, 40
- Brott I., et al., 2011, *A&A*, **530**, A115
- Cidale L. S., et al., 2012, *A&A*, **548**, A72
- Currie T., et al., 2010, *ApJS*, **186**, 191
- Davies B., Oudmaijer R. D., Sahu K. C., 2007, *ApJ*, **671**, 2059
- de Jager C., 1998, *A&ARv*, **8**, 145
- de Jager C., Nieuwenhuijzen H., 1997, *MNRAS*, **290**, L50
- Ekström S., et al., 2012, *A&A*, **537**, A146
- El Eid M. F., Champagne A. E., 1995, *ApJ*, **451**, 298
- Gesicki K., 1992, *A&A*, **254**, 280
- Gorlova N., Lobel A., Burgasser A. J., Rieke G. H., Ilyin I., Stauffer J. R., 2006, *ApJ*, **651**, 1130
- Hassenstein W., 1934, *Astronomische Nachrichten*, **253**, 457
- Humphreys R. M., 1978, *ApJS*, **38**, 309
- Humphreys R. M., Davidson K., 1994, *PASP*, **106**, 1025
- Humphreys R. M., Davidson K., Grammer S., Kneeland N., Martin J. C., Weis K., Burggraf B., 2013, *ApJ*, **773**, 46
- Humphreys R. M., Gordon M. S., Martin J. C., Weis K., Hahn D., 2017, *ApJ*, **836**, 64
- Israelian G., Lobel A., Schmidt M. R., 1999, *ApJ*, **523**, L145
- Jura M., Kleinmann S. G., 1990, *ApJ*, **351**, 583
- Klochkova V. G., Panchuk V. E., Tavolzhanskaya N. S., Usenko I. A., 2014, *Astronomy Reports*, **58**, 101
- Klochkova V. G., Panchuk V. E., Tavolzhanskaya N. S., 2018, *Astronomy Reports*, **62**, 623
- Kovtyukh V. V., 2007, *MNRAS*, **378**, 617
- Kraus M., 2009, *A&A*, **494**, 253
- Kraus M., Krügel E., Thum C., Geballe T. R., 2000, *A&A*, **362**, 158
- Kraus M., Borges Fernandes M., de Araújo F. X., 2010, *A&A*, **517**, A30
- Kraus M., et al., 2015, *A&A*, **581**, A75
- Kraus M., et al., 2016, *A&A*, **593**, A112
- Kraus M., et al., 2017, *AJ*, **154**, 186
- Lagadec E., Zijlstra A. A., Oudmaijer R. D., Verhoelst T., Cox N. L. J., Szczerba R., Mékarnia D., van Winckel H., 2011, *A&A*, **534**, L10
- Lambert D. L., Hinkle K. H., Hall D. N. B., 1981, *ApJ*, **248**, 638
- Liermann A., Kraus M., Schnurr O., Fernandes M. B., 2010, *MNRAS*, **408**, L6

- Liermann A., Schnurr O., Kraus M., Kreplin A., Arias M. L., Cidale L. S., 2014, *MNRAS*, **443**, 947
- Lobel A., 1997, PhD thesis, Ph.D. Dissertation, Vrije Univ. Brussel, ISBN: 978-90-423-0014-9
- Lobel A., de Jager C., Nieuwenhuijzen H., Smolinski J., Gesicki K., 1994, *A&A*, **291**, 226
- Lobel A., Israelian G., de Jager C., Musaev F., Parker J. W., Mavrogiorgou A., 1998, *A&A*, **330**, 659
- Lobel A., et al., 2003, *ApJ*, **583**, 923
- Maravelias G., Kraus M., Cidale L. S., Fernandes M. B., Arias M. L., Curé M., Vasilopoulos G., 2018, *MNRAS*,
- Mauron N., Josselin E., 2011, *A&A*, **526**, A156
- Muratore M. F., Kraus M., Oksala M. E., Arias M. L., Cidale L., Borges Fernandes M., Liermann A., 2015, *AJ*, **149**, 13
- Nickeler D. H., Goedbloed J. P., Fahr H.-J., 2006, *A&A*, **454**, 797
- Nickeler D. H., Wiegmann T., Karlický M., Kraus M., 2014, *ASTRA Proceedings*, **1**, 51
- Nieuwenhuijzen H., de Jager C., 1995, *A&A*, **302**, 811
- Oksala M. E., Kraus M., Arias M. L., Borges Fernandes M., Cidale L., Muratore M. F., Curé M., 2012, *MNRAS*, **426**, L56
- Oksala M. E., Kraus M., Cidale L. S., Muratore M. F., Borges Fernandes M., 2013, *A&A*, **558**, A17
- Oudmaijer R. D., Davies B., de Wit W.-J., Patel M., 2009, in Luteromoser D. G., Smith B. J., Stencel R. E., eds, *Astronomical Society of the Pacific Conference Series Vol. 412, The Biggest, Baddest, Coolest Stars*. p. 17 ([arXiv:0801.2315](https://arxiv.org/abs/0801.2315))
- Panchuk V. E., Klochkova V. G., Yushkin M. V., 2017, *Astronomy Reports*, **61**, 820
- Percy J. R., Kolin D. L., Henry G. W., 2000, *PASP*, **112**, 363
- Popper D. M., 1947, *AJ*, **52**, 129
- Raskin G., et al., 2011, *A&A*, **526**, A69
- Ryans R. S. I., Dufton P. L., Rolleston W. R. J., Lennon D. J., Keenan F. P., Smoker J. V., Lambert D. L., 2002, *MNRAS*, **336**, 577
- Sargent W. L. W., 1961, *ApJ*, **134**, 142
- Schuster M. T., Humphreys R. M., Marengo M., 2006, *AJ*, **131**, 603
- Sheffer Y., Lambert D. L., 1986, *PASP*, **98**, 914
- Shenoy D., et al., 2016, *AJ*, **151**, 51
- Simón-Díaz S., Herrero A., Uytterhoeven K., Castro N., Aerts C., Puls J., 2010, *ApJ*, **720**, L174
- Slechtsa M., Skoda P., 2002, *Publications of the Astronomical Institute of the Czechoslovak Academy of Sciences*, **90**, 1
- Stothers R. B., Chin C.-w., 2001, *ApJ*, **560**, 934
- Takeda Y., Takada-Hidai M., 1994, *PASJ*, **46**, 395
- Thackeray A. D., 1948, *MNRAS*, **108**, 279
- Tiffany C., Humphreys R. M., Jones T. J., Davidson K., 2010, *AJ*, **140**, 339
- Torres A. F., Cidale L. S., Kraus M., Arias M. L., Barbá R. H., Maravelias G., Borges Fernandes M., 2018, *A&A*, **612**, A113
- Wheelwright H. E., de Wit W. J., Weigelt G., Oudmaijer R. D., Ilee J. D., 2012, *A&A*, **543**, A77
- Yamamuro T., Nishimaki Y., Motohara K., Miyata T., Tanaka M., 2007, *PASJ*, **59**, 973
- Zsoldos E., Percy J. R., 1991, *A&A*, **246**, 441

This paper has been typeset from a $\text{\TeX}/\text{\LaTeX}$ file prepared by the author.

APPENDIX A: SELECTED LINE PROFILES

In this section we highlight the line-profile variability for selected lines. The lines are grouped such that Figures A1, A2, and A3 display lines of low, intermediate, and high excitation potential, respectively. Figure A4 presents the variability in H α , and Figure A5 compares the persistent emission in [Ca II] λ 7324 with the occasional emission in Fe I λ 6359.

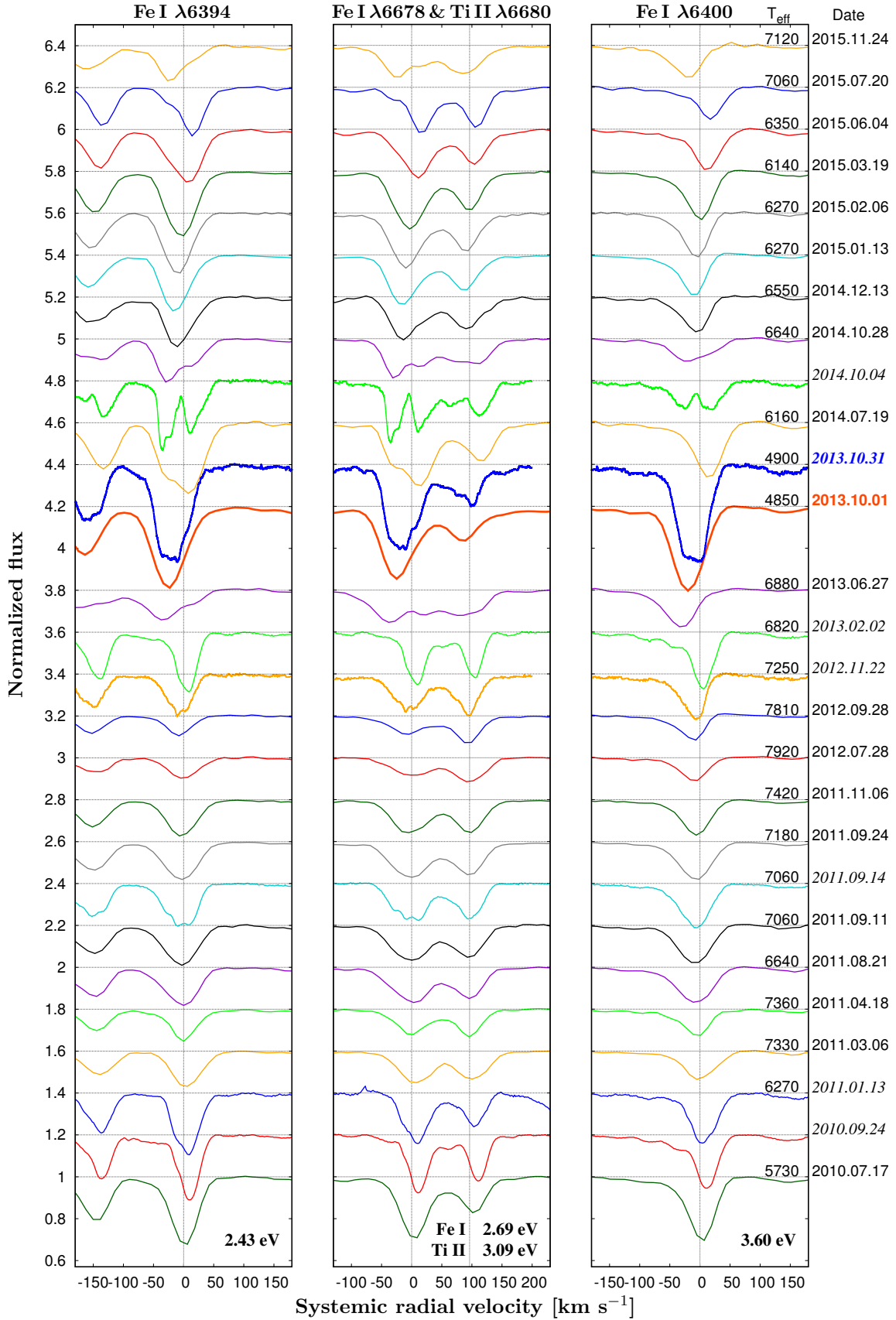


Figure A1. Variability in the profiles of selected low-excitation lines in the years 2010 – 2015. The excitation potentials are indicated. For easier comparison, the lines from the same observing date are shown in the same color.

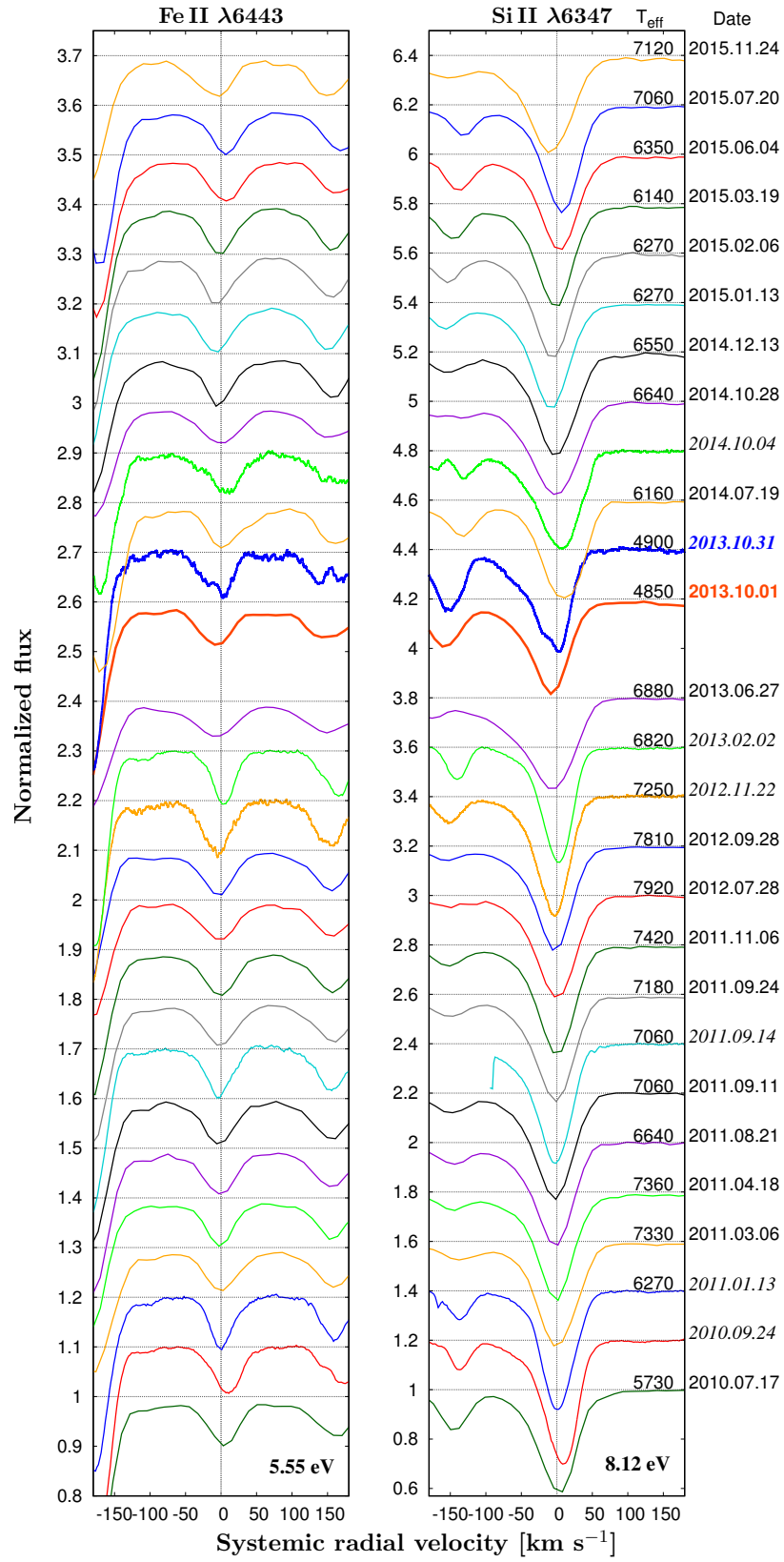


Figure A2. As Figure A1 but for medium-excitation lines.

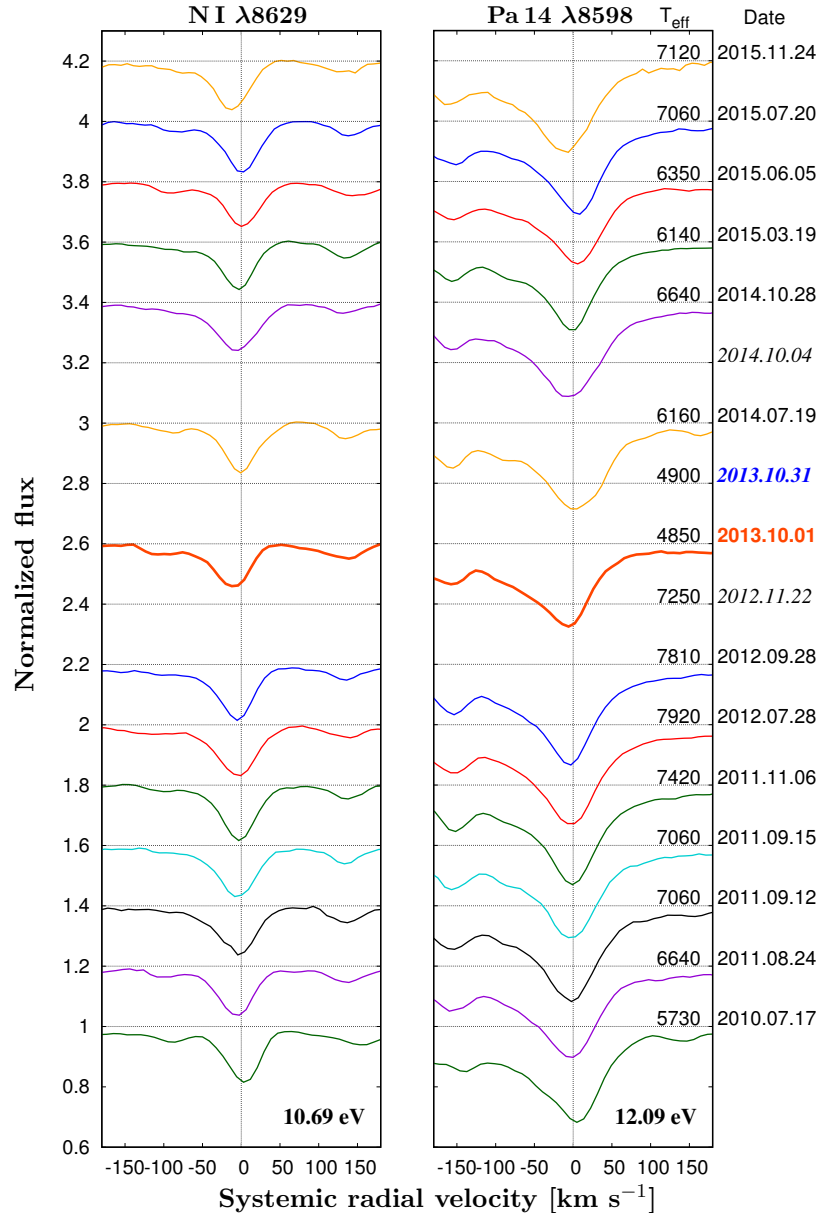


Figure A3. As Figure A1 but for high-excitation lines.

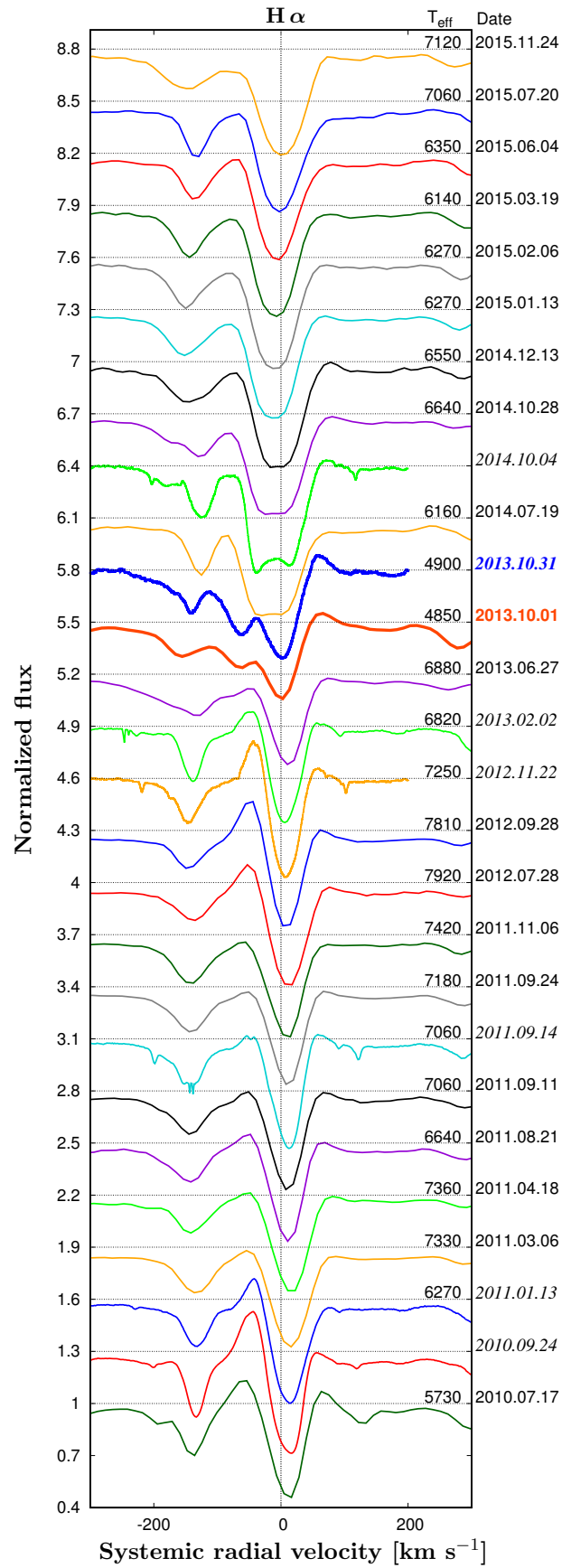


Figure A4. Variability in $H\alpha$.

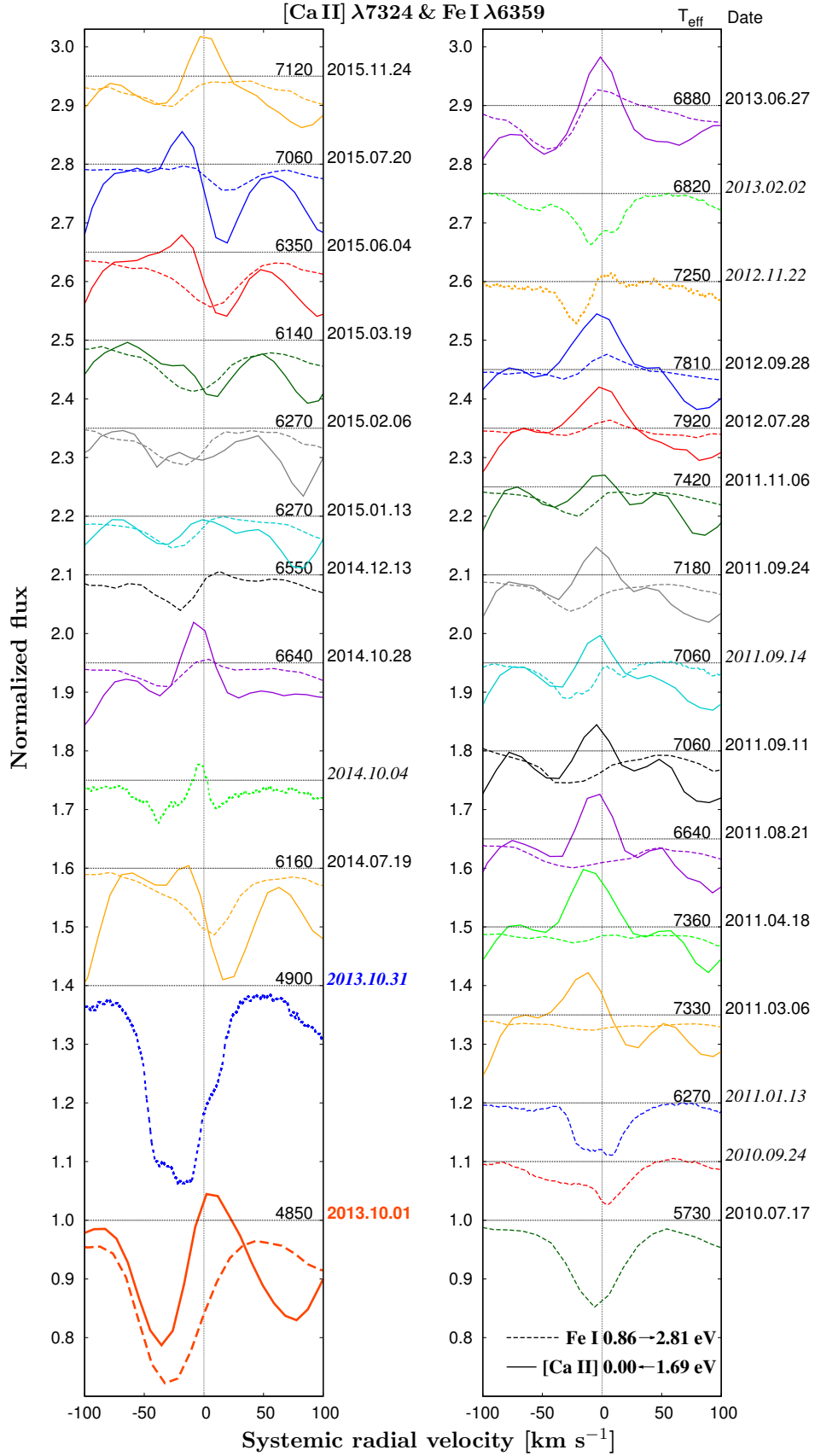


Figure A5. Variability in position and intensity of the [Ca II] λ 7324 emission line (solid lines) and the Fe I λ 6359 emission line (dashed lines) indicating their synchronous behavior.